



Published in final edited form as:

*J Med Chem.* 2009 April 9; 52(7): 2060–2066. doi:10.1021/jm900007a.

## Crystal Structures of Constitutive Nitric Oxide Synthases in Complex with *De Novo* Designed Inhibitors

Jotaro Igarashi<sup>†,%</sup>, Huiying Li<sup>†</sup>, Joumana Jamal<sup>†</sup>, Haitao Ji<sup>‡</sup>, Jianguo Fang<sup>‡</sup>, Graham R. Lawton<sup>‡</sup>, Richard B. Silverman<sup>‡</sup>, and Thomas L. Poulos<sup>†,\*</sup>

<sup>†</sup>Departments of Molecular Biology and Biochemistry, Pharmaceutical Sciences, and Chemistry University of California, Irvine, CA 92697-3900

<sup>‡</sup>Department of Chemistry, Department of Biochemistry, Molecular Biology, and Cell Biology, Center for Drug Discovery and Chemical Biology, Northwestern University, Evanston, IL 60208-3113

### Abstract

New nitric oxide synthase (NOS) inhibitors were designed *de novo* with knowledge gathered from the studies on the nNOS-selective dipeptide inhibitors. Each of the new inhibitors consists of three fragments: an aminopyridine ring, a pyrrolidine, and a tail of various length and polarity. The *in vitro* inhibitory assays indicate good potency and isoform selectivity for some of the compounds. Crystal structures of these inhibitors bound to either wild type or mutant nNOS and eNOS have confirmed design expectations. The aminopyridine ring mimics the guanidinium group of L-arginine and functions as an anchor to place the compound in the NOS active site where it hydrogen bonds to a conserved Glu. The rigidity of the pyrrolidine ring places the pyrrolidine ring nitrogen between the same conserved Glu and the selective residue nNOS Asp597/eNOS Asn368 which results in similar interactions observed with the  $\alpha$ -amino group of dipeptide inhibitors bound to nNOS. These structures provide additional information to help in the design of inhibitors with greater potency, physico-chemical properties, and isoform selectivity.

### Introduction

Three different mammalian isoforms of nitric oxide synthase (NOS) have been isolated and characterized: neuronal (nNOS), inducible (iNOS), and endothelial (eNOS). Although different isoforms have different cell and tissue distribution and are regulated through various mechanisms, they all catalyze the conversion of one guanidinium N atom of L-arginine (L-Arg) to nitric oxide. All three isoforms share a similar domain architecture with a N-terminal domain consisting of the catalytic heme active site and a cofactor, tetrahydrobiopterin, binding site, while the C-terminal domain containing FMN, FAD, and NADPH binding sites serves as an electron donating domain<sup>1,2</sup>. The linker between the two functional domains is a calmodulin binding motif. The binding of calmodulin enables electron flow from the flavins to the heme<sup>3</sup>.

Nitric oxide is an important signaling molecule involved in a wide range of physiological functions in the neuronal, immune, and cardiovascular system<sup>4,5</sup>. In order to exert appropriate functions, NO generation by the three different NOS isoforms is under tight regulation. The overproduction of NO by nNOS (or iNOS) and the underproduction by

\*CORRESPONDING AUTHOR: address here; Phone: 949-824-7020; Fax: 949-824-328; poulos@uci.edu..

<sup>%</sup>Present address: Institute of Multidisciplinary Research for Advanced Materials, Tohoku University 2-1-1 Katahira, Aoba-ku, Sendai 980-8577, Japan

eNOS have been shown to lead to pathophysiological conditions such as neurodegenerative diseases<sup>6</sup>, stroke<sup>7,8</sup>, rheumatoid arthritis<sup>9</sup>, hypertension<sup>10</sup>, and atherosclerosis<sup>11</sup>. Inhibition of nNOS (or iNOS) can thus be of considerable therapeutic benefit. However, inhibition must be isoform selective so that only NO formation by the disease-associated NOS, (e.g. nNOS) will be inhibited by the treatment while the physiological function of the other isoform, often eNOS, is unaffected. Isoform-selective inhibition is a challenging problem given that the three isoforms have very few differences in their three-dimensional structures.

Previous structure-activity studies in our laboratories on a series of *N*<sup>0</sup>-nitro-L-arginine containing dipeptide inhibitors<sup>12,13</sup> (Fig. 1A) have uncovered some key structural features in the NOS active site that are responsible for the selective binding affinity of these inhibitors to nNOS over eNOS<sup>14–17</sup>. Most importantly, the single amino acid difference, Asp597 in nNOS and Asn368 in eNOS, had been identified as the major reason why inhibitors **1**, **2** and **3** (Fig. 1A) bind more tightly to nNOS than eNOS. In nNOS these inhibitors adopt a curled binding mode which places the inhibitor  $\alpha$ -amino group between Asp597 and Glu592 for optimal electrostatic stabilization. Since eNOS has Asn368 rather than Asp, there is no energetic incentive for the inhibitor to curl, and instead the inhibitors adopt an extended conformation. One obvious design principle to emerge from this work is to have a positively charged group corresponding to the  $\alpha$ -amino group in **1**, **2** or **3** on a rigid scaffold such that the inhibitor will not have to curl in order to optimize charge interactions with Asp597 and Glu592. One other design principle is to replace the nitro-guanidinium group with an aminopyridine primarily because the aminopyridine should mimic the H-bonding pattern of the nitro-guanidinium while the pKa of the aminopyridine group ( $\approx 6 - 7$ ) should increase bioavailability<sup>18, 19</sup>. Based on these design principles, a new *de novo* design method was proposed, and a series of new inhibitors, **4**, **5**, **6**, and **7** (Fig. 1B), have been synthesized, the *in vitro* inhibitory potency determined, and the inhibitors applied to an animal model<sup>18,19</sup>. Here we report the crystal structures of these inhibitors bound to both eNOS and nNOS. Unfortunately we were unable to obtain suitable crystals of eNOS in complex with **4** or **5** which often is the case for inhibitors that bind poorly to eNOS.

## Results

### Binding of **4** and **5** to nNOS

Although all the new inhibitors **4** through **7** (Fig. 1A) used for crystallographic studies are the racemic mixture, the electron density of all four inhibitor complex structures show that only one enantiomer in each case is bound in the NOS active site. As expected, the two nitrogen atoms of the aminopyridine moiety of both **4** and **5** are involved in H-bonding with the Glu592 carboxylate (Fig. 2) similar to the bifurcated H-bonding found between two guanidino nitrogens of dipeptide inhibitor and the Glu592 side chain oxygens in the nNOS dipeptide complex structures<sup>12</sup>. The pyridine ring is roughly parallel to and stacking against the heme plane with the closest distance from the C3 atom of pyridine to the NB atom of heme in the range of 3.3 – 3.4 Å. The rigid pyrrolidine ring indeed brings its nitrogen within H-bonding distance to the Glu592 side chain resembling the curled binding conformation of dipeptide inhibitor where the  $\alpha$ -amino group forms a H-bond to Glu592. This sp<sup>3</sup>-hybridized nitrogen cation also forms a H-bond with the conserved structural water, which then forms H-bonding interactions with the selective residue Asp597 of nNOS. There are two hydrogen atoms attached to this nitrogen atom. One forms a H-bond with Glu592. Another one forms a H-bond with a conserved structural water which then forms H-bond interactions with Asp597. The amino group next to the pyrrolidine ring (N8 in Fig 2), mimicking the peptide amide nitrogen in the dipeptide inhibitor, makes a direct H-bond with the heme propionate group of pyrrole ring A. The tails of compounds **4** and **5** adopt quite different conformations. The amino group of **5** curls back to make a H-bond to the second heme propionate while the hydroxyl group of **4**, owing to its one carbon longer arm, can no longer make any direct

contact with the heme (Fig. 2). This additional charge-charge interaction between the terminal amine of **5** and heme propionate is probably a major factor contributing to the tighter binding of inhibitor **5** ( $K_i = 0.388 \mu\text{M}$ ) compared to **4** ( $K_i = 9.4 \mu\text{M}$ ).

### Binding of **6** and **7** to nNOS

Inhibitors **6** and **7** were derived from **5** with two modifications (Fig. 1A). First, a methyl group was introduced in the aminopyridine ring to provide additional contacts with a small hydrophobic pocket surrounded by Val567 and Phe584. Second, a chlorobenzyl group was attached to the terminal amino position in order to reach into a region where different NOS isoforms start to show sequence diversity. Inhibitor **6**, similar to **4** and **5**, has a (3'S, 4'S) *cis*-conformation at the two chiral carbons on the pyrrolidine ring. Its aminopyridine and pyrrolidine rings, therefore, bind to the active site the same as **4** and **5**, as described previously<sup>19</sup> (Fig. 3A). Inhibitor **7**, on the other hand, possesses a (3'R, 4'S) *trans*-conformation. However, the H-bonding interactions from both its aminopyridine and pyrrolidine rings to the Glu592 side chain are still retained (Fig. 3B). The newly added methyl group in both **6** and **7** makes van der Waals contact with Phe384 with a closest distance of 3.6Å. Larger differences between **6** and **7** are seen in the third fragment beyond the pyrrolidine ring. The 3'S conformation in the pyrrolidine of **6** places the neighboring amino group (N8 in Fig. 3) downward towards the heme where it H-bonds with the heme propionate (Fig. 3A), whereas the 3'R conformation in **7** brings N8 away from the propionate (Fig. 3B). Lack of this H-bond in **7** might be one of the reasons **7** ( $K_i = 0.25 \mu\text{M}$ ) binds more poorly to nNOS than does **6** ( $K_i = 0.085 \mu\text{M}$ ). The remaining chain leads the chlorophenyl moiety to a hydrophobic pocket defined by Met336, Leu337, Tyr706, and Trp306 of the neighboring subunit. However, the exact orientation of the chlorophenyl ring is somewhat ambiguous owing to the poor density quality in the region, especially in the structure of the **7** complex.

### Binding of **6** and **7** to eNOS

As expected, inhibitors **6** and **7** bind very much the same to eNOS. Part of the inhibitor design effort was to rigidify the inhibitor such that the key amino group interacting with Asp597 in nNOS would bind the same in eNOS<sup>18,19</sup>. This is exactly what happens. The pyrrolidine N atom is positioned the same in both eNOS and nNOS even to the extent that in both NOS isoforms a water molecule bridges between the pyrrolidine N atom and Asp597 in nNOS (Asn368 in eNOS). However, the pyrrolidine N atom should experience greater electrostatic stabilization in nNOS since nNOS has two negative charges nearby, Asp597 and Glu592, while eNOS has only Glu363. A second difference involves the chlorophenyl tail. In nNOS the aromatic ring can potentially form closer contacts with Met336 compared to the smaller corresponding residue, Val 106, in eNOS. However, the electron density for the chlorophenyl group is more well-ordered in eNOS than in nNOS and thus, it is doubtful that differences in interaction between the inhibitor aromatic ring and protein is a major contributor to isoform selectivity. The primary source of the 1,000-fold selectivity is more likely due to the greater electrostatic stabilization to the pyrrolidine N atom of **6** in nNOS.

### Inhibitor binding to the nNOS Asp597Asn/Met336Val mutant

In previous work we converted Asp597 and Met336 in nNOS to the corresponding residues in eNOS, Asn and Val, in order to test our hypothesis that both of these residues form more favorable contacts with the dipeptide inhibitors in nNOS than in eNOS<sup>13</sup>. Consistent with the finding that the binding mode of the new inhibitors reported here is unchanged between nNOS and eNOS, they also maintain the identical binding mode when wild type and mutant nNOS structures are compared. Inhibitor **5** found in the nNOS Asp597Asn/Met336Val double mutant structure has its aminopyridine and pyrrolidine rings H-bonded to Glu592 in a manner similar to that observed in wild type nNOS (Fig. 5). The only difference is that the

terminal amino group in the mutant structure has weak density and seems not to form a H-bond with the heme propionate from pyrrole ring D in contrast to the case in the wild type nNOS-5 complex structure. As expected, the  $K_i$  values for the nNOS double mutant increase for all inhibitors but the mutant still binds these inhibitors better than eNOS. Although we were not able to obtain suitable crystals of the eNOS-5 complex, it is probably safe to assume that 5 forms a complex with eNOS very similar to the one observed in nNOS and the nNOS double mutant. What then needs to be explained is why wild type nNOS binds 5 about 1,070-fold better than eNOS but only 90-fold better than the nNOS double mutant, a difference of 11-fold in  $K_i$ . In terms of free energy a factor of 11 accounts to  $\approx 1.4$  kcal/mol. It is possible that the tail primary amino group may be the source of this difference. In the wild type nNOS structure the primary amino group of 5 has strong and continuous electron density with a heme propionate, but this is not the case in the nNOS double mutant. An even weaker interaction between this amino group and the heme propionate in eNOS could easily account for 1.4 kcal/mol.

### MM-PBSA to estimate $\Delta G$ of binding

It would be advantageous to employ a rapid computational method to estimate which inhibitors not only bind best but exhibit greater selectivity for nNOS over eNOS. Toward this end we have been using the MM-PBSA methodology as implemented in Amber 9.0 to compute  $\Delta G_{\text{bind}}$ . The procedure described in Materials and Methods was used to compute  $\Delta G_{\text{bind}}$  for four different NOS inhibitors in five different crystal structures. As shown in Fig. 6A these are all aminopyridine inhibitors similar to inhibitors used for the crystal structures described in this study. However, because the  $K_i$  values from which  $\Delta G_{\text{exp}}$  are derived for inhibitors 4, 5, 6, and 7 used in the present study are mixtures of optical isomers, these were not included in the training set for generating Fig. 6B. Fig. 6B is a plot of computed free energy obtained from single energy minimized structures<sup>20,21</sup> vs. experimental free energies derived from  $K_i$  measurements. The computed free energies are much larger since we have not included inhibitor entropy corrections. Even so, the fit is quite good. Although the inhibitors used in Fig. 6 are very similar, they span a  $K_i$  range of over  $10^3$ , yet the relative  $\Delta G_{\text{calc}}$  agrees well with  $\Delta G_{\text{exp}}$ .

Inhibitors 4 and 5 were used with the plot in Fig. 6B as test cases. Since we do not have crystal structures of these inhibitors bound to eNOS, 4 and 5 were modeled into the eNOS active site pocket assuming that they adopt the same binding mode as in nNOS.  $\Delta G_{\text{calc}}$  was calculated using the protocol outlined in the Methods section and converted to the same scale as experimental,  $\Delta G_{\text{exp}}$ , using the straight line equation derived from Fig. 6B.

$$\Delta G_{\text{calc}} (\text{corrected}) = (\Delta G_{\text{calc}} + 12.12) / 6.55$$

$\Delta\Delta G$  is defined as the difference in binding free energy between nNOS and eNOS,  $\Delta\Delta G = \Delta G_{\text{bind}}(\text{nNOS}) - \Delta G_{\text{bind}}(\text{eNOS})$ . For inhibitor 4  $\Delta\Delta G_{\text{exp}} = 2.2$  kcal/mol and  $\Delta\Delta G_{\text{calc}} = 1.3$  kcal/mol while for 5  $\Delta\Delta G_{\text{exp}} = 4.2$  kcal/mol and  $\Delta\Delta G_{\text{calc}} = 4.1$  kcal/mol (Table 1). It thus appears that the simplified MM-PBSA method used here is capable of correctly estimating NOS isoform selectivity and should prove useful in pre-screening novel NOS inhibitors of similar structure.

## Discussion

The present work illustrates that fairly simple design principles derived from our previous work<sup>12, 22</sup> can be used to prepare novel NOS inhibitors that retain isoform selectivity but might exhibit improved pharmacological properties. As in the earlier dipeptide inhibitor work, the key to isoform selectivity is the Asp597 (nNOS) vs. Asn368 (eNOS) difference.

The pyrrolidine ring N atom and its close proximity to two negative charges in the nNOS active site compared to only one negative charge in the eNOS active site appears to be the key factor controlling selectivity. The advantage of these newer pyrrolidine inhibitors is that they are fairly rigid compared to the dipeptide inhibitors used in our previous work, and all bind the same to eNOS and nNOS; therefore, understanding the structural basis for selectivity is not complicated by differences in inhibitor conformation as in the case of the dipeptide inhibitors. The simplified MM-PBSA procedure, where only a single energy minimized structure is used and entropic factors ignored, does a reasonably good job in estimating isoform selectivity and is very rapid.

The ultimate practical outcome of these efforts is to develop therapeutic agents that can treat neuro-pathological conditions associated with the overproduction of NO by nNOS. Very recently, our groups have shown that compounds closely related to **6** are capable of significant protection against neural damage in a rabbit cerebral palsy model<sup>19</sup>. Moreover, protection is associated with a decrease in brain NO production and brain NOS activity without affecting eNOS regulated blood pressure. Our efforts on NOS structure-based drug design thus add to a short but growing documented list where the close interaction between structural biology, medicinal chemistry, and computer modeling can result in the development of novel compounds with demonstrated *in vivo* therapeutic effects.

## Experimental Section

### Protein and crystal preparations

The full-length, wild type or mutant, nNOS and eNOS proteins were expressed in *E. coli* strain BL21 (DE3). The proteins were purified with Ni Sepharose and/or 2', 5'- ADP Sepharose columns as described previously<sup>12, 13, 23</sup>. The heme domain nNOS or eNOS was generated from the partially purified full-length enzymes by limited trypsin digest. The heme domain protein was further separated from the fragments of the reductase domain by gel filtration through a Superdex 200 column<sup>23</sup>.

The purified nNOS or eNOS heme domain protein was concentrated to 7–9 (nNOS) or 20 (eNOS) mg/ml. About 8–10 mM of inhibitor was added to the protein before the sitting drop vapor diffusion crystallization setups using the reservoir solutions reported earlier<sup>12, 13, 23</sup>. Crystallization plates were left in a 5 °C incubator for more than 2 days to allow crystals to reach full size. Fresh crystals of less than 10 days old were flash-cooled with liquid nitrogen after passing through a series of cyroprotectant solutions as described previously<sup>12, 13, 23</sup>.

### Inhibitory assays

Nitric oxide formation was monitored by the hemoglobin capture assay<sup>24</sup> with buffer components described previously<sup>25</sup>. The apparent  $K_i$  values were obtained by measuring percent inhibition in the presence of 10  $\mu$ M L-arginine with various amount of inhibitor. The parameters of the following inhibition equation were fitted to the initial 1 min velocity data: % inhibition =  $100[I]/\{[I] + K_i (1 + [S]/K_m)\}$ .  $K_m$  value for nNOS double mutant was determined to be 1.9  $\mu$ M.

### X-ray diffraction data collection and crystal structure determination

The X-ray diffraction data were collected under a liquid nitrogen stream (100 K) with CCD detectors either at Stanford Synchrotron Radiation Lightsource (SSRL, Menlo Park, CA) or at Advanced Light Source (ALS, Berkeley, CA). Raw data were processed with HKL2000<sup>26</sup>. The binding of inhibitor was detected by difference Fourier synthesis. The inhibitor then was modeled into the density using O<sup>27</sup> and refined with CNS<sup>28</sup>. Water molecules were added automatically with CNS and inspected visually in O. The refined

structures were validated before deposition to the RSCB data bank (<http://deposit.pdb.org/validate/>). The data collection and refinement statistics are summarized in Table 2.

### Computational approaches

The free energy of binding of various NOS inhibitors was estimated using the MM-PBSA method<sup>29</sup> as implemented in Amber 9.0. In this method the total free energy of the NOS-inhibitor complex is taken as the sum of the following energy terms

$$G = G_{MM} + G_{solv} + G_{np} + TS_{solute}$$

where  $E_{MM}$  = the total molecular mechanics energy computed with the Sander module in Amber 9.0,  $G_{solv}$  is the solvation free energy estimated from the Poisson-Boltzman equation,  $G_{np}$  = the nonpolar solvation energy estimated from the solvent accessible surface area, and  $TS_{solute}$  = the solute entropy. From a single energy minimized structure the free energy was computed for the NOS-inhibitor complex, NOS alone with the inhibitor removed, and the inhibitor alone. The overall free energy of binding was computed from the following equation

$$\Delta G_{bind} = (G_{complex} - G_{receptor} - G_{inhibitor})$$

As others have done the solute entropy was ignored<sup>30</sup>. Given that the inhibitors used for these calculations are structurally very similar with a similar number of rotatable bonds, ignoring inhibitor entropy introduces little error in comparing relative calculated and experimental free energies but does, of course, preclude the calculation of absolute free energies.

Inhibitor parameters and charges were assigned using the GAFF force field<sup>31</sup> and AM1-BCC charge scheme<sup>32,33</sup> as implemented in the Antechamber module in Amber 9.0. Heme parameters developed for cytochrome P450 were provided by Dr. Dan Harris<sup>34</sup>. It was necessary to carefully check the Antechamber output to make sure the correct atom types were assigned. For some inhibitors it was necessary to increase the force constant on improper torsion angles from 1.1 to 10.1 kcal/Å in order to maintain planarity of the nitroguanidinium and aminopyridine groups. To prepare the models for energetic calculations all crystallographic waters were removed and TIP3 waters added back within 30 Å of the inhibitor. The resulting solvated structure was first energy minimized using the steepest descent method for 1,000 cycles with the inhibitor and heme heavy atom restrained to the starting crystallographic positions. The restraints were relaxed to 10.0 kcal/Å<sup>2</sup> for the inhibitor and heme followed by another 1,000 cycles of refinement. In the last step the restraints for the heme and inhibitor were relaxed to 1.0 kcal/Å<sup>2</sup> followed by 1,000 cycles of minimization. In the case of some eNOS-inhibitor complexes where structures were not determined but the nNOS-inhibitor complex structure was available, the inhibitor was positioned into the eNOS active site assuming it adopts the same conformation and position as that found in nNOS.

### Acknowledgments

This research was supported by NIH grants GM57353 (T.L.P) and GM49725 (R.B.S.). We thank the beam line staff at SSRL and ALS for their assistance during data collections.

## Abbreviations used

<b>NOS</b>	nitric oxide synthase
<b>nNOS</b>	neuronal NOS
<b>iNOS</b>	inducible NOS
<b>eNOS</b>	endothelial NOS
<b>2',5'-ADP</b>	adenosine 2',5'-diphosphate
<b>CCD</b>	charge coupled device
<b>MM-PBSA</b>	Molecular Mechanics with Poisson-Boltzman Surface Area methodology
<b>GAFF</b>	general Amber force field
<b>AM1-BCC</b>	Austin Model 1-Bond Charge Correction. Crystallographic coordinates have been deposited with the Protein Data Base with accession codes 3B3M, 3B3N, 3B3O, 3B3P, 3DQR, 3DQS, and 3DQT

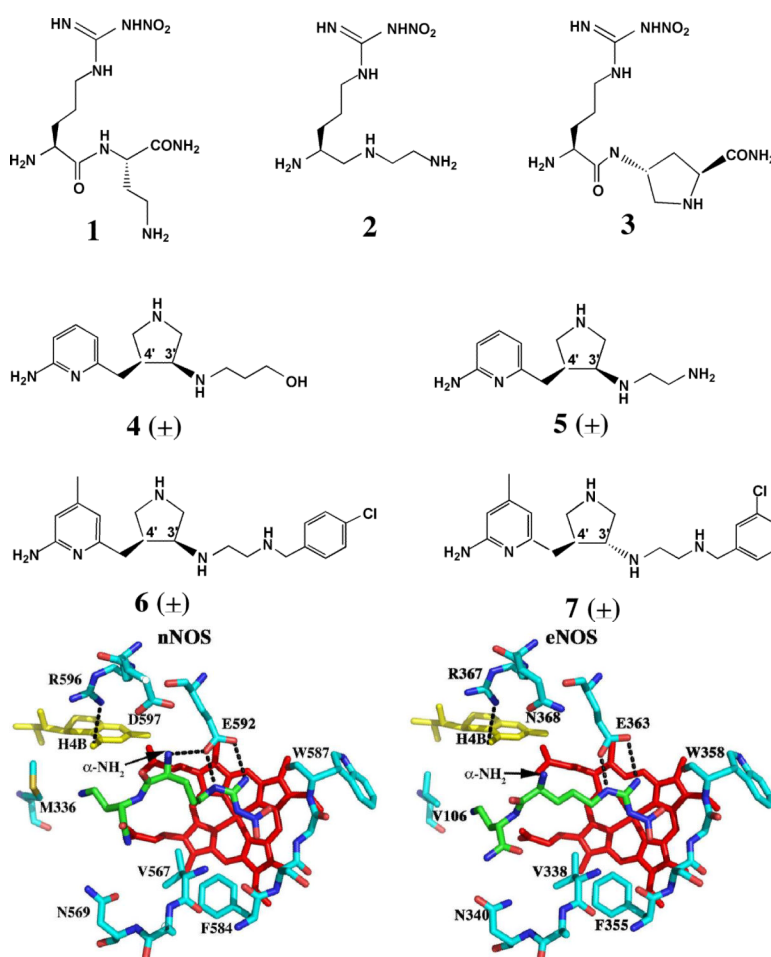
## References

1. Griffith OW, Stuehr DJ. Nitric oxide synthases: properties and catalytic mechanism. *Annu. Rev. Physiol.* 1995; 57:707–736. [PubMed: 7539994]
2. Raman, CS.; Martasek, P.; Masters, BSS. Structural themes determining function in nitric oxide synthases. In: Kadish, KM.; Smith, KM.; Guillard, R., editors. *The porphyrin handbook*. Vol. Vol. 4. Academic Press; San Diego: 2000. p. 293-339.
3. Abu-Soud HM, Stuehr DJ. Nitric oxide synthases reveal a role for calmodulin in controlling electron transfer. *Proc. Natl. Acad. Sci. U. S. A.* 1993; 90:10769–10772. [PubMed: 7504282]
4. Moncada S, Palmer RM, Higgs EA. Nitric oxide: physiology, pathophysiology, and pharmacology. *Pharmacol. Rev.* 1991; 43:109–142. [PubMed: 1852778]
5. Kerwin JF Jr, Lancaster JR Jr, Feldman PL. Nitric oxide: a new paradigm for second messengers. *J. Med. Chem.* 1995; 38:4343–4362. [PubMed: 7473563]
6. Dawson VL, Dawson TM. Nitric oxide in neurodegeneration. *Prog. Brain Res.* 1998; 118:215–229. [PubMed: 9932444]
7. Lipton P. Ischemic cell death in brain neurons. *Physiol. Rev.* 1999; 79:1431–1568. [PubMed: 10508238]
8. Sims NR, Anderson MF. Mitochondrial contributions to tissue damage in stroke. *Neurochem. Int.* 2002; 40:511–526. [PubMed: 11850108]
9. Bingham CO 3rd. The pathogenesis of rheumatoid arthritis: pivotal cytokines involved in bone degradation and inflammation. *J. Rheumatol. Suppl.* 2002; 65:3–9.
10. Taddei S, Virdis A, Ghiadoni L, Sudano I, Salvetti A. Endothelial dysfunction in hypertension. *J. Cardiovascular Pharmacol.* 2001; 38(Suppl. 2):S11–S14.
11. Napoli C, de Nigris F, Williams-Ignarro S, Pignalosa O, Sica V, Ignarro LJ. Nitric oxide and atherosclerosis: An update. *Nitric Oxide.* 2006; 15:265–279. [PubMed: 16684613]
12. Flinspach ML, Li H, Jamal J, Yang W, Huang H, Hah JM, Gomez-Vidal JA, Litzinger EA, Silverman RB, Poulos TL. Structural basis for dipeptide amide isoform-selective inhibition of neuronal nitric oxide synthase. *Nat. Struct. Mol. Biol.* 2004; 11:54–59. [PubMed: 14718923]
13. Li H, Flinspach ML, Igarashi J, Jamal J, Yang W, Gomez-Vidal JA, Litzinger EA, Huang H, Erdal EP, Silverman RB, Poulos TL. Exploring the binding conformations of bulkier dipeptide amide inhibitors in constitutive nitric oxide synthases. *Biochemistry.* 2005; 44:15222–15229. [PubMed: 16285725]
14. Huang H, Martasek P, Roman LJ, Masters BS, Silverman RB. N(omega)-Nitroarginine-containing dipeptide amides. Potent and highly selective inhibitors of neuronal nitric oxide synthase. *J. Med. Chem.* 1999; 42:3147–3153. [PubMed: 10447959]

15. Huang H, Martasek P, Roman LJ, Silverman RB. Synthesis and evaluation of peptidomimetics as selective inhibitors and active site probes of nitric oxide synthases. *J. Med. Chem.* 2000; 43:2938–2945. [PubMed: 10956202]
16. Hah JM, Roman LJ, Martasek P, Silverman RB. Reduced amide bond peptidomimetics. (4S)-N-(4-amino-5-[aminoalkyl]aminopentyl)-N'-nitroguanidines, potent and highly selective inhibitors of neuronal nitric oxide synthase. *J. Med. Chem.* 2001; 44:2667–2670. [PubMed: 11472219]
17. Gomez-Vidal JA, Martasek P, Roman LJ, Silverman RB. Potent and selective conformationally restricted neuronal nitric oxide synthase inhibitors. *J. Med. Chem.* 2004; 47:703–710. [PubMed: 14736250]
18. Ji H, Stanton BZ, Li H, Martasek P, Roman L, Poulos TL, Silverman RB. Minimal pharmacophoric elements and a pharmacophore-driven strategy for fragment-based de novo design, an approach directed at molecular diversity and isozyme selectivity. design of selective neuronal nitric oxide synthase inhibitors. *J. Am. Chem. Soc.* 2008; 130:3900–3914. [PubMed: 18321097]
19. Ji H, Tan S, Igarashi J, Li H, Derrick M, Martasek P, Roman LJ, Vasquez-Vivar J, Poulos TL, Silverman RB. Selective neuronal nitric oxide synthase inhibitors and the prevention of cerebral palsy. *Ann. Neurol.* 2008 in press.
20. Kuhn B, Gerber P, Schulz-Gasch T, Stahl M. Validation and use of the MMPBSA approach for drug discovery. *J. Med. Chem.* 2005; 48:4040–4048. [PubMed: 15943477]
21. Weis A, Katebzadeh K, Soderhjelm O, Nilsson I, Ryde U. Ligand affinities predicted with the MM/PBSA method: Dependence on the simulation method and the force field. *J. Med. Chem.* 2006; 49:6596–6606. [PubMed: 17064078]
22. Flinspach M, Li H, Jamal J, Yang W, Huang H, Silverman RB, Poulos TL. Structures of the neuronal and endothelial nitric oxide synthase heme domain with D-nitroarginine-containing dipeptide inhibitors bound. *Biochemistry.* 2004; 43:5181–5187. [PubMed: 15122883]
23. Li H, Shimizu H, Flinspach M, Jamal J, Yang W, Xian M, Cai T, Wen EZ, Jia Q, Wang PG, Poulos TL. The novel binding mode of N-alkyl-N'-hydroxyguanidine to neuronal nitric oxide synthase provides mechanistic insights into NO biosynthesis. *Biochemistry.* 2002; 41:13868–13875. [PubMed: 12437343]
24. Hevel JM, Marletta MA. Nitric-oxide synthase assays. *Methods Enzymol.* 1994; 233:250–258. [PubMed: 7516999]
25. Hah JM, Martasek P, Roman LJ, Silverman RB. Aromatic reduced amide bond peptidomimetics as selective inhibitors of neuronal nitric oxide synthase. *J. Med. Chem.* 2003; 46:1661–1669. [PubMed: 12699384]
26. Otwinowski Z, Minor W. Processing of X-ray diffraction data collected in oscillation mode. *Methods Enzymol.* 1997; 276:307–326.
27. Jones TA, Zou J-Y, Cowan SW, Kjeldgaard M. Improved methods for building models in electron density and the location of errors in these models. *Acta Crystallogr.* 1991; A47:110–119.
28. Brunger AT, Adams PD, Clore GM, DeLano WL, Gros P, Grosse-Kunstleve RW, Jiang J-S, Kuszewski J, Nilges M, Pannu NS, Read RJ, Rice LM, Simonson T, Warren GL. Crystallography & NMR System: A new software suite for macromolecular structure determination. *Acta Crystallogr.* 1998; D54:905–921.
29. Massova I, Kollman PA. Computational alanine scanning to probe protein-protein interactions: A novel approach to evaluate binding free energies. *J. Am. Chem. Soc.* 1999; 121:8133–8143.
30. Brown SP, Muchmore SW. High-throughput calculation of protein-ligand binding affinities: Modification and adaption of the MM-PBSA protocol to enterprise grid computing. *J. Chem. Inf. Model.* 2006; 46:999–1005. [PubMed: 16711718]
31. Wang J, Wolf RM, Caldwell JW, Kollman PA, Case D. Development and testing of a general Amber force field. *J. Am. Chem. Soc.* 2004; 25:1157–1174.
32. Jakalian A, Bush BL, Jack DB, Bayly CI. Fast, efficient generation of high-quality atom charges. AM1-BCC model: I. Method. *J. Comp. Chem.* 2000; 21:132–146.
33. Jakalian A, Jack DB, Bayly CI. Fast, efficient generation of high-quality atom charges. AM1-BCC model: II. Parameterization and validation. *J. Comp. Chem.* 2002; 23:1623–1641. [PubMed: 12395429]



34. Harris DL, Park JY, Gruenke L, Waskell L. Theoretical study of the ligand-CYP2B4 complexes: Effect of structure on binding free energies and heme spin state. *Proteins*. 2004; 15:895–914. [PubMed: 15146488]

**Fig. 1.**

**A)** Chemical structures and nomenclature for the inhibitors discussed in the paper. **1.** L-*N*<sup>0</sup>-nitroarginine-2,4-L-diaminobutyramide; **2.** (4*S*)-*N*-(4-amino-5-[aminoethyl]aminopentyl)-*N'*-nitroguanidine; **3.** L-*N*<sup>0</sup>-nitroarginine-(4*R*)-amino-L-proline amide; **4.** (±)-3-{*cis*-4'-[(6''-aminopyridin-2''-yl)methyl]pyrrolidin-3'-ylamino}propan-1-ol; **5.** (±)-*N*<sup>1</sup>-{*cis*-4'-[(6''-aminopyridin-2''-yl)methyl]pyrrolidin-3'-yl}ethane-1,2-diamine; **6.** (±)-*N*<sup>1</sup>-{*cis*-4'-[(6''-amino-4''-methylpyridin-2''-yl)methyl]pyrrolidin-3'-yl}-*N*<sup>2</sup>-(4'-chlorobenzyl)ethane-1,2-diamine; **7.** (±)-*N*<sup>1</sup>-{*trans*-4'-[(6''-amino-4''-methylpyridin-2''-yl)methyl]pyrrolidin-3'-yl}-*N*<sup>2</sup>-(3'-chlorobenzyl)ethane-1,2-diamine. **B)** Structure of **1** complexed to nNOS and eNOS<sup>12</sup>. In nNOS the inhibitor adopts a curled conformation in order to enable the inhibitor α-amino group to optimally interact with both Glu592 and Asp597. In eNOS the residue corresponding to Asp597 is Asn368 and as a result, the inhibitor adopts an extended conformation.

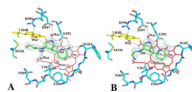


**Fig. 2.**

Active site structures of the wild type nNOS with inhibitor **4** (panel A) or **5** (panel B) bound viewed side by side in an identical orientation. Shown also the  $F_o - F_c$  omit map contoured at  $3.0\sigma$  for each inhibitor. Hydrogen bonds are drawn with the dashed lines. The atomic color scheme for amino acids is: carbon, cyan or green; nitrogen, blue; oxygen, red; sulfur, yellow. The figures are made with PyMol (<http://pymol.sourceforge.net>).

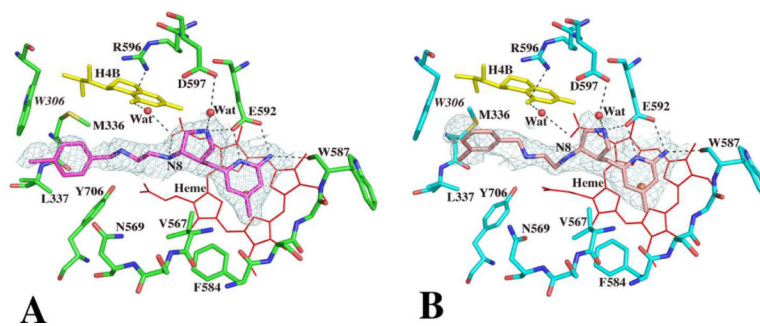


**Fig. 3.** Active site structures of the wild type nNOS with inhibitor **6** (panel A) or **7** (panel B) bound. Density around each inhibitor is the  $F_o - F_c$  omit map contoured at  $3.0\sigma$ . Residue Trp306 belongs to the neighboring subunit.

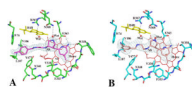


**Fig. 4.** Active site structures of the wild type eNOS with inhibitor **6** (panel A) or **7** (panel B) bound. Also shown around the inhibitor is the  $F_o - F_c$  omit map contoured at  $3.0\sigma$ . Residue Trp76 belongs to the neighboring subunit. Alternate conformations of heme propionate off the pyrrole ring D are also depicted.



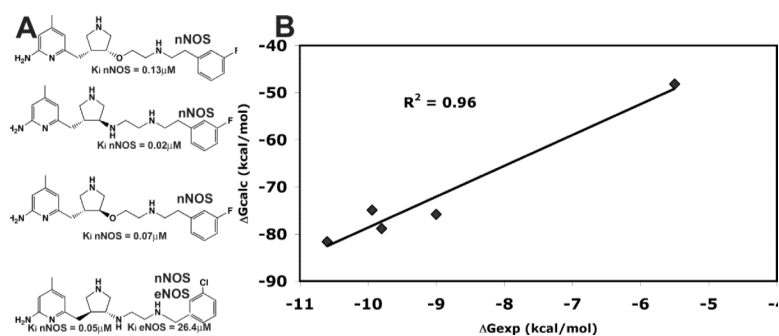


**Fig. 6.** A) Structures of the various inhibitors complexed with either eNOS, nNOS, or both used to construct the plot in panel B. B) Plot of experimental  $\Delta G_{\text{exp}}$  vs computed  $\Delta G_{\text{calc}}$  using 5 different crystal structures.

Table 1

*In vitro* NOS inhibition ( $K_i$  in  $\mu\text{M}$ )

Inhibitor	nNOS	eNOS	nNOS/DM	eNOS/mNOS	$\Delta\Delta G_{\text{exp}}$ (kcal/mol)	$\Delta\Delta G_{\text{calc}}$ (kcal/mol)
<b>1</b>	0.3	107.0		357		
<b>2</b>	0.15	80.0		533		
<b>3</b>	0.10	110.0		1100		
4( $\pm$ )	9.4	366.6	49.2	39	2.2	1.3
5( $\pm$ )	0.388	416.7	36.7	1068	4.2	4.1
6( $\pm$ )	0.085	85.2	1.2	1002	-	-
7( $\pm$ )	0.25	95.2	6.1	381	-	-



Table 2

Data collection and refinement statistics

Data set <sup>1</sup>	PDB code	nNOS 4 3B3M	nNOS 5 3B3N	nNOS 6 3B3O	nNOS 7 3B3P	nNOS DM 5 3DQR	eNOS 6 3DQS	eNOS 7 3DQT
Cell dimensions(Å) (SG: P2 <sub>1</sub> 2 <sub>1</sub> 2 <sub>1</sub> )		a = 51.50 b = 109.53 c = 163.25	a = 52.05 b = 110.69 c = 164.84	a = 52.21 b = 111.53 c = 164.84	a = 52.58 b = 110.25 c = 164.39	a = 51.87 b = 110.70 c = 164.36	a = 57.96 b = 106.84 c = 156.77	a = 58.25 b = 106.49 c = 156.42
Data resolution (Å)		1.95	1.98	2.05	2.45	2.40	2.03	2.54
Total observations		279484	245363	217270	131153	155390	261113	140776
Unique reflections		65107	66436	60556	35031	37670	64663	32771
R <sub>sym</sub> <sup>2</sup>		0.040 (0.251) <sup>3</sup>	0.064 (0.532)	0.052 (0.428)	0.101 (0.592)	0.094 (0.732)	0.054 (0.504)	0.089 (0.740)
<I/σ >		15.9 (5.1) <sup>3</sup>	11.7 (1.9)	10.7 (1.9)	6.3 (1.6)	7.2 (1.9)	9.6 (2.1)	9.2 (2.1)
Completeness (%)		94.9 (65.1) <sup>3</sup>	98.7 (90.1)	97.8 (96.1)	98.7 (99.4)	99.3 (99.0)	99.9 (100.0)	99.6 (99.9)
Reflection used in refinement		64931	66359	60120	34892	37621	63716	32770
R factor <sup>4</sup>		0.204	0.230	0.213	0.209	0.205	0.197	0.197
R-free <sup>5</sup>		0.233	0.270	0.253	0.265	0.261	0.227	0.258
No. protein atoms		6663	6659	6677	6677	6819	6418	6439
No. heterogen atoms		165	163	181	181	163	209	199
No. water molecules		546	392	418	247	268	488	184
bond length(Å)		0.007	0.009	0.010	0.009	0.010	0.009	0.010
bond angle (°)		1.4	1.5	1.4	1.5	1.5	1.5	1.6

<sup>1</sup> nNOS DM refers to nNOS D597N/M336V double mutant. See Fig. 1A for chemical structures and nomenclature of inhibitors.<sup>2</sup> R<sub>sym</sub> =  $\sum |I - \langle I \rangle| / \sum I$ , where I is the observed intensity of a reflection and  $\langle I \rangle$  the averaged intensity of multiple observations of the reflection and its symmetry mates.<sup>3</sup> The values in parentheses were obtained in the outermost resolution shell.<sup>4</sup> R factor =  $\sum ||F_o| - |F_c|| / \sum |F_o|$ , F<sub>o</sub> and F<sub>c</sub> are the observed and calculated structure factors, respectively.<sup>5</sup> R-free was calculated with the 5% of reflections set aside randomly throughout the refinement.